

inspection of the implications and assumptions of the theory developed here are also forthcoming. Finally, work to document the effect of swelling on birefringence using the model developed in this paper will be reported in an upcoming paper.

Acknowledgment. I thank Professors W. L. Mattice and B. E. Erman for their valuable comments. Many thanks are also due to Doreen d'Auteuil for meticulously typing the manuscript.

References and Notes

- (1) Mark, J. E.; Erman, B. *Rubberlike Elasticity: A Molecular Primer*; Wiley-Interscience: New York, 1988.
- (2) Queslel, J. P.; Mark, J. E. In *Comprehensive Polymer Science*; Allen, G., Ed.; Pergamon Press: Oxford, 1988.
- (3) Galiatsatos, V.; Mark, J. E. *Macromolecules* **1987**, *20*, 2631.
- (4) Galiatsatos, V.; Mark, J. E. *Polym. Bull.* **1987**, *17*, 197.
- (5) Galiatsatos, V.; Mark, J. E. In *Advances in Silicon-Based Polymer Science*; Ziegler, J., Fearon, G., Eds.; American Chemical Society: Washington, DC, 1989.
- (6) Erman, B.; Flory, P. J. *Macromolecules* **1983**, *16*, 1601.
- (7) Lieberman, M. H.; Abe, Y.; Flory, P. J. *Macromolecules* **1972**, *5*, 550.
- (8) Kuhn, W.; Gr \ddot{u} n, F. *Kolloid-Z.* **1942**, *101*, 248.
- (9) Volkenstein, M. W. *Configurational Statistics of Polymeric Chains*; Timasheff, S. N., Timasheff, M. J., Eds.; Interscience: New York, 1963; Chapter 7.
- (10) Treloar, L. R. G. *The Physics of Rubber Elasticity*, 3rd ed.; Clarendon Press: Oxford, 1975; Chapter 9.
- (11) Flory, P. J. *Statistical Mechanics of Chain Molecules*; Interscience: New York, 1969.
- (12) Flory, P. J. *J. Chem. Phys.* **1977**, *66*, 5720.
- (13) Erman, B.; Flory, P. J. *Macromolecules* **1982**, *15*, 806.
- (14) Erman, B.; Monnerie, L. *Macromolecules* **1989**, *22*, 3342.
- (15) Erman, B.; Kloczkowski, A.; Mark, J. E. *Macromolecules* **1989**, *22*, 1432.
- (16) Kloczkowski, A.; Mark, J. E.; Erman, B. *Macromolecules* **1989**, *22*, 1423.
- (17) Pearson, D. S. *Macromolecules* **1977**, *10*, 696.
- (18) Ullman, R. *J. Chem. Phys.* **1979**, *71*, 436.
- (19) Ullman, R. *Macromolecules* **1982**, *15*, 1393.

A One-Component Model for the Phase Behavior of Dispersions Containing Associative Polymers

Maria M. Santore, William B. Russel,* and Robert K. Prud'homme

Department of Chemical Engineering, Princeton University, Princeton, New Jersey 08544

Received October 10, 1989; Revised Manuscript Received February 16, 1990

ABSTRACT: The statistical mechanical theory developed herein predicts the effects of associative polymer, random walk chains with adhesive end groups, on the interaction between parallel plates at full and restricted equilibrium conditions. The Derjaguin approximation and Barker-Henderson perturbation theory then determine interparticle potentials and macroscopic thermodynamic variables, respectively, with the compositions of coexisting phases following from classical thermodynamic criteria for equilibrium in one-component systems. Weakly or nonassociative polymers induce depletion attractions that result in reversible phase transitions. Increasing the strength of the adhesion to the plates diminishes the range and strength of the attraction, so higher polymer concentrations are needed to induce flocculation. Sufficient adsorption to the plates may cause a repulsive barrier that stabilizes dispersions against depletion flocculation at full equilibrium. Strong adsorption, however, results in a bridging attraction that grows with polymer concentration until the surface is saturated and then diminishes with additional polymer. This leads to flocculation at low polymer concentrations and restabilization at a higher value that depends on the solvent quality. The interactions at restricted equilibrium mimic the long-range features of the full equilibrium potentials but contain an additional repulsive core.

Introduction

The role of polymers in dispersion stability and phase behavior has been a topic of interest for a number of years. Conventional systems contain homopolymers that induce phase separations via either of two mechanisms, depending on the polymer's affinity for the particle surface. It is well established both experimentally¹⁻⁴ and theoretically^{1,5-7} that nonadsorbing polymer causes a volume restriction attraction and reversible phase transitions. With adsorbing homopolymers the precise mechanism for bridging flocculation remains unclear, with the most obvious explanations relying on kinetic rather than purely equilibrium effects.⁸

Our interests center on the phase behavior induced by the addition of hydrophobically modified water-soluble

polymers to stable colloidal dispersions. These polymers consist of nonadsorbing water-soluble chains with grafted hydrocarbon arms (10-20 carbons long), comprising 1-2 wt % of the molecule. In aqueous solvents, the hydrophobes associate intra- and intermolecularly and adsorb reversibly onto the surface of hydrophobic particles.⁹ Hydrophobically modified polymers comprise the state of the art for thickeners in the coatings industry, but their commercial use is limited by a poor understanding of their effects on the equilibrium properties of dispersions, due to the specificity of the hydrophobe adsorption. The work presented here applies not only to these new paint thickeners but also to specialty polymers employed in enhanced oil recovery and biomedical applications.

Traditionally, aqueous coatings included nonadsorbing high molecular weight polymers such as (hydroxyethyl)-

cellulose (HEC)⁹ to enhance the rheology of latex paints. Difficulties with the classical formulations include spatter and brush marks, which Sperry et al.⁹ attributed to the microscopically phase separated nature of the dispersions. Indeed, the nonadsorbing polymer induces volume restriction flocculation, a phenomenon conceived by Asakura and Oosawa⁶ and later documented experimentally by de Hek and Vrij¹⁰ with silica particles in polystyrene solutions. With aqueous latices Sperry² observed rigid flocs with particles large relative to the polymer molecules and fluidlike flocs when the polymer size approached the particle diameter. Gast⁵ and, more recently, Vincent¹ explained the nature of the phase transition in terms of the range of the particle-particle interaction, comparing experiments with HEC-latex systems³ and poly(dimethylsiloxane) in silica dispersions¹ to theoretical treatments of spheres interacting via osmotic attractions. Their pseudo-one-component models ascribe all effects of polymer and solvent to the interparticle potential and provide the base line for the associative thickener model presented here.

Previous theories¹¹⁻¹⁴ determined the effects of adsorbing and nonadsorbing homopolymer on the forces between two flat plates immersed in a polymer solution. These models first resolve the segment distribution near the surface in order to calculate free energies and, hence, the flat-plate interaction potentials. Asakura and Oosawa⁶ showed that nonadsorbing macromolecules excluded from the region between the two plates produce an attractive osmotic force between the plates, with a range comparable to the chain dimension. When the polymer adsorbs to the surface, the range of the interaction depends on the thickness of the adsorbed layers. Since tails may extend fairly far from the surface, as determined by scaling,¹⁵ lattice,¹² and mean field^{14,16} theories, the interaction between the plates may be rather long range, observed by Luckham and Klein¹⁷ to commence beyond $7R_g$ for poly(ethylene oxide) on mica. For strict thermodynamic equilibrium, de Gennes¹³ predicts attractions between the plates, since at very small separations the entropic loss of the polymer should exceed any energetic contributions to its chemical potential, driving the polymer from the gap and giving an osmotic attraction.

These effects of adsorbing and nonadsorbing homopolymer on flat-plate interactions provide a backdrop for our treatment of associatively modified polymer, i.e., polymer containing adsorbing groups (or "stickers") along a non-adsorbing backbone. Certainly, in the limit of exceptionally weak stickers, associative polymer should behave as a non-adsorbing chain. Likewise, with many hydrophobes, an associative macromolecule should act as an adsorbing homopolymer. Between these extremes, however, we expect behavior different from either case. For example, with a few hydrophobes of significant adsorption strength on each chain, the adsorbed layer at low coverage should consist of isolated, effectively grafted coils, in contrast to a homopolymer either adsorbed flat against the surface or completely depleted. However, the reversibility of adsorption for hydrophobically modified polymers may result in different interaction potentials than with grafted coils.

Indeed, Sperry⁹ noted that hydrophobically modified poly(ethylene oxide) imparts unusual phase behavior to latex dispersions. At low polymer concentrations a phase separation interpreted as bridging flocculation occurs, but at higher polymer concentrations the system appears to restabilize. Seen through a microscope, the particles in the latter lack Brownian motion, indicating a network

structure. At moderate surfactant concentrations (in addition to the polymer), phase separation is observed at all but the lowest polymer concentrations. This is understood as volume restriction flocculation, since the surfactant may saturate hydrophobic interactions, preventing adsorption onto the latices.

In an attempt to corroborate Sperry's interpretation of phase behavior induced by associative polymers, we presented a two-component statistical mechanical treatment of these dispersions.¹⁸ The actual system consisting of solvent, polymer, and latices was modeled as a binary mixture of hard spheres and random walk chains containing associative end groups. From the probabilities that this simple polymer would achieve a free or adsorbed/associated configuration, we calculated polymer-polymer and polymer-particle potentials whose topology was sensitive to sticker strength and placement and the backbone molecular weight. Barker-Henderson perturbation theory and classical thermodynamics facilitated predictions of phase behavior. Fluid-fluid phase transitions resulted for systems with primarily repulsive polymer-particle interactions; however, even the weakest attraction shifted the phase boundary to higher polymer concentrations, indicating a stabilizing trend consistent with Sperry's observation of volume restriction flocculation when hydrophobic interactions are saturated by surfactant. The binary model, however, does not predict the bridging flocculation arising from adsorption of the grafted arms onto the latices, perhaps because explicit three-body interactions, i.e., particle-polymer-particle, were not included.

In this work, we permit bridged configurations between parallel plates in addition to configurations addressed in the binary mixture model, at the cost of assuming a constant polymer concentration in the fluid around the particles. Additional elements include a finite hydrophobe size that allows calculation of surface coverages and adsorbed amounts, an extension to nonideal backbones, and a restricted equilibrium calculation (originally conceived by de Gennes¹⁹) for strongly adsorbed chains. As two spheres approach at full equilibrium, the polymer partitions between the interstitial ("gap") region and bulk polymer solution to maintain equal polymer chemical potentials. It is unclear how often this situation occurs experimentally, as the time scale of Brownian collisions may be shorter than the time for desorption. Alternately, in the restricted equilibrium scenario, we assume that adsorbed polymer is trapped and compressed in the gap as the particles approach, while free polymer exits with the solvent.

The model presented in this work focuses primarily on the effects of single polymer coils on the interparticle potential, neglecting intercoil associations, and hence micellization. Experiments²⁰ indicate such associations, even in dilute solution; however, this is an especially difficult problem in the context of the one-component approach. Our binary model addresses this issue by predicting the effect of hydrophobe strength on the limit of stability for a solution of reversibly interacting coils. Unstable solutions either form micelles or contain insoluble polymer. Hence in the one-component approach, one might consider the potential between plates immersed in a polymer solution where single chains maintain equilibrium with a micelle phase. The micelles might simply constrain the free polymer concentration; however, the effects of micelle-plate and micelle-micelle interactions are beyond our speculation. Hence in this paper, we restrict ourselves to the chains that undergo internal but not coil-coil associations.

We first develop the flat-plate interaction potentials, which are then used to calculate the phase behavior of the dispersion. Predictions are compared to the trends observed by Sperry⁹ and will be used in a subsequent paper to interpret our own experiments.

Interaction Potentials

This section describes the statistical mechanical formulation of interaction potentials between two flat plates in a polymer solution. As the plates move together from infinite separation, the polymer partitions between the gap and bulk solution under either full or restricted equilibrium conditions. In the gap, chains may adsorb to the surfaces in a variety of configurations, including bridging. Hydrophobes act as spatial δ functions in free solution (i.e., no adhesion is felt until the chain end is exactly on the plate); but in contrast to our previous work, adsorbed stickers have a finite dimension, which limits coverage on the plates.

Through the Derjaguin approximation, flat-plate potentials are converted to sphere-sphere interactions proportional to the particle/polymer diameter ratio. Barker-Henderson perturbation theory applied to these interactions then translates microscopic information into macroscopic variables, in this case, Helmholtz free energy. Equating pressures and particle chemical potentials in all phases identifies fluid-fluid and fluid-solid phase transitions.

Chain Statistics. The interaction is determined by the properties of the dissolved polymer, a random-walk or nonideal chain with adhesive end groups, or "stickers". These stickers may associate inter- or intramolecularly (with adhesion energy u_{pp}) or adsorb reversibly (with adhesion energy u_{pw}) to occupy a finite region on the plates.

The sticker strength depends on the length of the hydrophobe. Though the exact relationship is unclear, Tanford's experiments²¹ suggest how adhesion strength relates to the number of carbons in a linear alkane chain:

$$\frac{\mu^\circ(\text{hydrocarbon}) - \mu^\circ(\text{water})}{kT} = -4.114 - 1.493 \times (\text{no. of carbons in chain}) \quad (1)$$

Equation 1 describes the energy to transfer one hydrocarbon chain from an aqueous to a bulk hydrocarbon phase and does not specifically pertain to micellization or adsorption. We expect the latter to involve a fraction, here assumed to be approximately 1/4, of the energy in (1) since only one side of the hydrophobe is involved in adsorption. Equation 1 then provides an approximate hydrophobe size for a specified sticker strength; the corresponding number of segments follows from equating the persistence length to approximately six C-C or C-O bonds,²² as for an alkane hydrophobe.

We treat the hydrophobes as δ functions in three-dimensional space (i.e., as points) but assign a hydrophobe containing s_0 statistical segments an area equal to l^2 , for each segment adsorbed. A mean field depending on the concentration of adsorbed segments describes the energy of adsorption to a surface with a fractional coverage ϕ_s . With χ_s as the adsorption energy onto a clean surface (defined as a positive number in units of kT), the incremental sticker adsorption developed in detail by Ploehn and others¹⁶ is

$$\frac{u_{pw}}{kT}(L) = -\chi_s + \frac{u_{pp}}{kT}\phi_s(L) - \ln(1 - \phi_s(L)) \quad (2)$$

L reminds us that these quantities depend on the distance between the plates. In the limit of zero coverage, the

sticker-wall adhesion, u_{pw} , approaches the sticker strength, χ_s , determined by its chemistry. However, as the surface fills, segment-segment interactions within the adsorbed layer affect the sticker-wall adhesion. For low and moderate surface coverages, the second term on the right-hand side provides additional attractive energy, but as the fractional coverage approaches unity, an infinite repulsion deriving from the third term prevents further adsorption. Note that ϕ_s is the fractional coverage of stickers contacting the surface, not the "equivalent monolayer" coverage used by other authors.^{11,16} It should be emphasized that only sticker segments, not nearby backbone segments, contribute to coverage and surface interactions.

The statistics of Markov processes determine the coil's configuration, with the individual segments subject to a mean field $U(\mathbf{R})$, depending on the local segment concentration, n , via the excluded volume parameter, ν , for pairwise interactions. The segment distribution function $P(s, \mathbf{R}|\mathbf{R}')$ for a coil between two plates satisfies (cf. Russel, Saville, and Schowalter²³)

$$\frac{\partial P(s, \mathbf{R}|\mathbf{R}')}{\partial s} = \frac{1}{6} \nabla^2 P(s, \mathbf{R}|\mathbf{R}') + N(1 - e^{U(\mathbf{R})/kT})P(s, \mathbf{R}|\mathbf{R}') \quad (3)$$

with

$$1 - e^{U(\mathbf{R})/kT} = -\nu n + \dots$$

s , the fractional distance along the chain contour; N , the number of segments in the chain; the \mathbf{R} and \mathbf{R}' , positions scaled on the end-to-end distance $N^{1/2}l$. $P(s, \mathbf{R}|\mathbf{R}')$ describes the probability of a chain starting at \mathbf{R}' having the N th segment at \mathbf{R} . The parallel-plate geometry is imposed through boundary conditions that $P(s, x|x')$ vanish for $x = 0$ and L , to ensure that no segments penetrate plates at separation L . The excluded volume, ν/l^3 , vanishes for ideal or random-walk chains, and for slightly nonideal chains (i.e., good solvent) is a small positive number, usually less than 0.1.

Dolan and Edwards²⁴ express solutions to eq 3 for ideal chains ($\nu = 0$) as expansions appropriate for plate separations small or large relative to the coil dimensions:

$$P(N, x|x') = \left(\frac{3}{2\pi}\right)^{1/2} \sum_{i=-\infty}^{\infty} \{\exp[-1.5(x - x' - 2iL)^2] - \exp[-1.5(x + x' - 2iL)^2]\} \quad \text{for } L \geq 0.75 \quad (4a)$$

$$P(N, x|x') = \frac{2}{L} \sum_{j=1}^{\infty} \sin \frac{j\pi x}{L} \sin \frac{j\pi x'}{L} \exp\left[\frac{-\pi^2 j^2}{L^2}\right] \quad \text{for } L \leq 0.75 \quad (4b)$$

No more than 5 ($i = j = 2$) terms are needed to match far- and near-field forms at $L = 0.75$.







Integrating the positions of the chain ends at x and x' over the gap or placing them at specific points in the gap determines the probabilities of configurations corresponding to bridging or adsorption to a single plate. When adsorbed, the stickers rest a distance $l/2$ inside the plates, as the boundary conditions specify $P(N, 0|x') = 0$. We are particularly interested in the configurations in Table I which correspond to specific energy states for the chain. Note that the adsorbed ring configuration is not shown since (2) incorporates sticker-sticker adhesions on the surface.

The partition function W , describing the configurations available to a coil as

$$W = \int P(N, \mathbf{R}|\mathbf{R}') e^{-U(\mathbf{R}, \mathbf{R}')/kT} d\mathbf{R} d\mathbf{R}' \quad (5)$$

Table I
Derivations of Probabilities of Important Configurations

A Coil Between Two Plates

Configuration	Expression
 (reference state)	$\text{norm}(\text{gap}) = 1 + P(N, R R) e^{-u_{pw}/kT}$ (same as polymer-wall)
	$P_0(L) = \frac{1}{\text{norm}} \int_0^L \int_0^L P(N, L, x x') dx, dx'$
	$P_1(L) = \frac{4}{\text{norm}} \int_0^L P(N, L, 1/2 x') dx'$
	$P_2(L) = \frac{2}{\text{norm}} P(N, L, 1/2 1/2)$
	$P_{L-1}(L) = \frac{2}{\text{norm}} P(N, L, 1/2 [L-1/2])$
	$P_0^{\text{Loop}}(L) = \frac{1}{\text{norm}} \int_0^L P(N, L, x x) dx$

simplifies for chains in the gap to

$$W_g = P_0 + P_1(e^{-u_{pw}/kT} - 1) + (P_2 + P_{L-1})(e^{-2u_{pw}/kT} - 1) + P_0^{\text{Loop}}(e^{-u_{pw}/kT} - 1) \quad (6)$$

since there are a finite number of energy states. W_g is normalized on a bulk solution including chains in a loop configuration.

In addition to the partition function, several other important quantities derive from the configuration probabilities in Table I, for example, fractional coverage ϕ_s :

$$\phi_s(L) = \frac{(4.5)6^{1/2}s_0}{\pi N} \frac{\phi_g L(L)}{W_g(L)} \left[\frac{1}{2} P_1(L)(e^{-u_{pw}/kT} - 1) + (P_2(L) + P_{L-1}(L))(e^{-2u_{pw}/kT} - 1) \right] \quad (7)$$

ϕ_g is the average volume fraction of chains in the gap, based on the radius of gyration R_g :

$$\phi_g = \frac{4\pi R_g^3 n_g}{3N} \quad (8)$$

with n_g the average segment density in the gap. The square-bracketed term in (7) describes the number of configurations involving adsorption, normalized on the configurations available to an unconstrained chain. Dividing by W_g gives the fraction of available configurations in the gap involving adsorption. The prefactor converts from adsorbed stickers per area to fractional coverage, using $R_g = N^{1/2}l/6^{1/2}$ for ideal coils.

The adsorbed amount, ϕ_a , measures the number of chains with ends adsorbed to either plate. For restricted equilibrium, this remains constant at the value at infinite separation:

$$\phi_a^\infty = \phi_p[(P_1 L)^\infty(e^{-u_{pw}^\infty/kT} - 1) + (P_2 L)^\infty(e^{-2u_{pw}^\infty/kT} - 1)] \quad (9)$$

with ϕ_p the polymer volume fraction in bulk solution, defined as in (8). Here, P_1^∞ and P_2^∞ are the infinite separation limits of the probabilities defined in Table I; that for bridging vanishes identically.

Interaction Potentials: General Derivation. The interaction potential between the two plates is the Helmholtz free energy per unit area for a system of constant volume containing the gap between the plates and the surrounding bulk solution, less a reference state where the plates are isolated:

$$\Phi_{fp} = \frac{A(L)}{\text{area}} - \frac{A(L \rightarrow \infty)}{\text{area}} \quad (10a)$$

Equation 10a requires the total Helmholtz free energy:

$$A(L) = A_g(L) + A_p(L) \quad (10b)$$

which includes contributions from the gap (g) and the bulk polymer solution (p), both of which depend on plate separation L . The Helmholtz free energy for a system of volume V containing M chains at temperature T is²³

$$\frac{A}{kT} = M \left(\ln \frac{n}{N} - 1 - \ln W \right) + \frac{1}{kT} \int \left(f - n \frac{\partial f}{\partial n} \right) dV \quad (11)$$

The first two terms on the right comprise the ideal limit, while the logarithm of W accounts for the internal degrees of freedom of the chain. The free energy density, f , arises from segment-segment interactions, and the integral derived by Helfand²⁵ corrects for the fact that mean field theory overcounts segment-segment interactions. For later reference, note that chemical potentials and pressure are related to the Helmholtz free energy by

$$\mu_c = \left(\frac{\partial A}{\partial M_c} \right)_{\Pi, M_p} \quad (12a)$$

$$\mu_p = \left(\frac{\partial A}{\partial M_p} \right)_{\Pi, M_c} \quad (12b)$$

$$\Pi = - \left(\frac{\partial A}{\partial V} \right)_{M_p, M_c} \quad (13)$$

with M the number of each species present and c and p denoting particle (colloid) and polymer, respectively.

Note that we have related the interaction potential to the total Helmholtz free energy of the system, in contrast to the approach taken by de Gennes¹⁹ and others.¹¹ These authors evaluate the surface tension, or excess free energy of the gap solution, at constant volume and pressure, which Evans²⁶ has shown requires a hydrostatic pressure correction as the plate separation varies. Our method implicitly includes the effect of the hydrostatic pressure since the total Helmholtz free energy accounts for both the gap and the bulk. Before substituting (11) and (13) into (10) to calculate the potential, we consider the components of the integral term in the gap and in the bulk, elaborating on the Helmholtz free energy.

The mean field description of excluded volume interactions defines f as

$$\frac{f}{kT} = \frac{\nu n^2}{2} + \dots + \frac{f_s}{kT} \quad (14)$$

which ν describes segment-segment interactions in the polymer solution and f_s accounts for adsorption to the plates. With ideal chains, $\nu = 0$, leaving only the surface contributions to the integral. With the energy to adsorb in incremental hydrophobe given by (2) and related to f_s by

$$\frac{\partial f_s}{\partial n_s} = \frac{u_{pw}}{s_0} \quad (15)$$

the integral in (11) becomes

$$-\int_{V_g} \frac{\nu}{2} n^2 d\mathbf{R} + \frac{A}{s_0 l^2} \left[\phi_s \left(1 - \frac{u_{pp}\phi_s}{2kT} \right) + \ln(1 - \phi_s) \right] \quad (16)$$

with A the plate area, and $s_0 l^2$ the area occupied by a hydrophobe. Recall that the second term in (16) vanishes when calculating the free energy of the bulk polymer solution.

Combining (11), (14), and (16) and substituting into (10b) give the total Helmholtz free energy as a function of plate separation:

$$\begin{aligned} \frac{A(L)}{kT} = & M_g(L) \left(\ln \frac{n_g(L)}{N} - 1 - \ln W_g(L) \right) - \\ & \int_{V_g} \left(\frac{\nu}{2} n^2(\mathbf{R}) \right) d\mathbf{R} + M_p \left(\ln \frac{n_p(L)}{N} - 1 - \ln W_p \right) - \\ & V_p \left(\frac{\nu}{2} n_p^2 \right) + \frac{A}{s_0 l^2} \left[\phi_s \left(1 - \frac{u_{pp}\phi_s}{2kT} \right) + \ln(1 - \phi_s) \right] \quad (17) \end{aligned}$$

with M_g and M_p the number of chains in the gap and bulk, respectively. At this stage, we have the option of imposing full or restricted equilibrium criteria to relate the bulk and gap concentrations.

Gaussian Coils. At full equilibrium, equation the polymer chemical potentials (12b) between the gap and the bulk determines the polymer concentration in the gap for Gaussian coils ($\nu = 0$) through

$$\phi_g = \frac{\phi_p W_g}{W_p} \exp \left[\phi_g \frac{\partial \ln W_g}{\partial \phi_g} - \phi_p \frac{\partial \ln W_p}{\partial \phi_p} - \frac{8\pi N}{6^{5/2} L s_0} \times \left(1 - \frac{u_{pp}\phi_s}{kT} - \frac{1}{1 - \phi_s} \right) \frac{\partial \phi_s}{\partial \phi_g} \right] \quad (18)$$

Substituting this into (17) and rearranging gives

$$\begin{aligned} \frac{A}{kT} \frac{Nl^2}{A} = & L \phi_g \left[-1 + \phi_g \frac{\partial \ln W_g}{\partial \phi_g} \right] + \\ & \frac{8\pi N}{6^{5/2} s_0} \left[\phi_s \left(1 - \frac{u_{pp}\phi_s}{2kT} \right) + \ln(1 - \phi_s) - \right. \\ & \left. \phi_g \frac{\partial \phi_s}{\partial \phi_g} \left(1 - \frac{u_{pp}\phi_s}{kT} - \frac{1}{1 - \phi_s} \right) \right] \quad (19) \end{aligned}$$

the total equilibrium Helmholtz free energy per area times Nl^2 . Since (18) is implicit in ϕ_g , both (18) and (19) must be solved together. The interaction potential results from (19) by subtracting its limit for infinite separation. This expression is consistent with Evans²⁶ calculations that account for the pressure distribution in the gap arising from a nonuniform concentration profile. (Note that (19) cannot be derived from surface tension alone.)

The restricted-equilibrium scenario recognizes that adsorbed polymer may not desorb and exit the gap on the time scale of particle collisions, constraining those chains adsorbed at infinite separation to remain in the gap even when their chemical potential exceeds the bulk solution. Adsorbed chains do, however, rearrange as the partition function W_g dictates. At large separations, free polymer penetrates the gap with $\mu_p = \mu_g$. As the plates approach, full equilibrium will be maintained as long as the gap contains free polymer, i.e.

$$\phi_g(\text{restrict}) = \phi_g(\text{equil}) \quad \text{if } \phi_g(\text{equil}) \geq \phi_a^\infty/L \quad (20a)$$

When the equilibrium requires desorption, restricted

conditions dictate

$$\phi_g(\text{restrict}) = \phi_a^\infty/L \quad \text{if } \phi_g(\text{equil}) < \phi_a^\infty/L \quad (20b)$$

Substituting (20b) into (17) and rearranging give the corresponding free energy per area times Nl^2

$$\begin{aligned} \frac{A^{\text{restrict}} Nl^2}{kTA} = & \phi_a^\infty \left[\ln \frac{\phi_a^\infty}{\phi_p W_g L} - 1 \right] + \\ & \frac{8\pi N}{6^{5/2} s_0} \left[\phi_s \left(1 - \frac{u_{pp}\phi_s}{kT} \right) + \ln(1 - \phi_s) \right] \quad (21) \end{aligned}$$

Parallel-plate potentials follow from subtracting the infinite separation limit of (19) from (21).

Nonideal Chains. Up to this point, we have derived parallel-plate interactions in solutions of ideal polymers only, neglecting segment-segment interactions, except on the plate surface. In dilute solutions with a good solvent such that $0 < \nu < l^3$, segment-segment repulsions expand coils and increase the osmotic pressure of the solution. The excluded volume interactions also perturb the chain distribution function from the Gaussian statistics P° , which satisfy

$$\frac{\partial P^\circ(s, x|x')}{\partial s} = \frac{1}{6} \nabla^2 P^\circ(s, x|x') \quad (22)$$

and the appropriate boundary conditions for the parallel-plate geometry or the bulk solution.

If segment-segment interactions alter the probability distribution function only slightly, we can write

$$\begin{aligned} P(s, \mathbf{R}|\mathbf{R}') = & P^\circ(s, \mathbf{R}|\mathbf{R}') - \nu N n_m P'(s, \mathbf{R}|\mathbf{R}') \\ = & P^\circ(s, \mathbf{R}|\mathbf{R}') - \tilde{\nu} N^{1/2} \phi_m P'(s, \mathbf{R}|\mathbf{R}') \quad (23) \end{aligned}$$

where $\tilde{\nu} = 3^{2.5} \nu / (2^{1/2} \pi)$ such that $\nu N n_m = \tilde{\nu} N^{1/2} \phi_m$, with the subscript m denoting the concentration at the middle of the gap. Then $\tilde{\nu} N^{1/2} \phi_m P'$ tallies the configurations excluded by segment-segment interactions. In the gap, the local segment distribution varies smoothly, making the solution of (3) quite difficult. Thus we assume a piecewise constant segment density profile based on δ , the adsorbed layer thickness for associative chains and the depletion layer for nonadsorbing homopolymer. The local segment concentration then takes only two values, ϕ_m for free chains in the center of the gap and ϕ_δ for adsorbed chains in the layers near the plates:

$$\phi_m = \frac{\phi_g}{W_g} \frac{P_0 L}{L - 2\delta} \quad \text{for } \delta < x < L - \delta \quad (24a)$$

$$\begin{aligned} \phi_\delta = & \frac{\phi_g}{W_g} \frac{L}{2\delta} [P_1(e^{-u_{pw}/kT} - 1) + (P_2 + P_{1-1})(e^{-2u_{pw}/kT} - 1)] \\ & \text{for } x < \delta \text{ or } x > L - \delta \quad (24b) \end{aligned}$$

These satisfy the mass balance

$$\phi_g = \frac{2\delta}{L} \phi_\delta + \frac{L - 2\delta}{L} \phi_m \quad (25)$$

Substituting (23) into (3) and subtracting (22) yields, to first order in $\tilde{\nu} N^{1/2} \phi(x)$

$$\frac{\partial P'(s, x|x')}{\partial s} = \frac{1}{6} \nabla^2 P'(s, x|x') + \frac{\phi(x)}{\phi_m} P^\circ(s, x|x') \quad (26)$$

A solution employing Green's functions gives

$$P(N, x|x') = P^0(N, x|x') - \tilde{\nu} N^{1/2} \phi_m \int_0^1 \int_{\delta}^{L-\delta} P^0(1-s, x^0|x) G(s, x'|x^0) dx^0 ds - \tilde{\nu} N^{1/2} \phi_\delta \int_0^1 \int_0^\delta P^0(1-s, x^0|x) G(s, x'|x^0) dx^0 ds - \tilde{\nu} N^{1/2} \phi_\delta \int_0^1 \int_{L-\delta}^L P^0(1-s, x^0|x) G(s, x'|x^0) dx^0 ds \quad (27)$$

which must be integrated numerically.

The probabilities of the various configurations and the partition function of a coil in the gap are calculated according to Table I and from (6), respectively. The segment-segment exclusion will affect the parallel-plate interaction (17) directly, through the integral of the segment profile, and indirectly, through the partition function. The average polymer volume fraction at full equilibrium in the gap, ϕ_g , is determined by equating chemical potentials from the gap and bulk regimes:

$$\phi_g = \frac{\phi_p W_g}{W_p} \exp \left\{ \phi_g \frac{\partial \ln W_g}{\partial \phi_g} - \phi_p \frac{\partial \ln W_p}{\partial \phi_p} + \tilde{\nu} N^{1/2} \left[\frac{L-2\delta}{L} \phi_m \frac{\partial \phi_m}{\partial \phi_g} + \frac{2\delta}{L} \phi_\delta \frac{\partial \phi_\delta}{\partial \phi_g} - \phi_p \right] \right\} \times \exp \left\{ - \left[\frac{8\pi N}{6^{2.5} L s_0} \left(1 - \frac{u_{pp} \phi_s}{kT} - \frac{1}{1-\phi_s} \right) \frac{\partial \phi_s}{\partial \phi_g} \right] \right\} \quad (28)$$

Substituting (24) and (25) into (17) yields a general expression for the Helmholtz free energy per area (times Nl^2) of a system with two plates of separation L immersed in a good polymer solution at dilute conditions:

$$\frac{A}{kT} \frac{Nl^2}{A} = L \phi_g \left[-1 + \phi_g \frac{\partial \ln W_g}{\partial \phi_g} - \phi_p \frac{\partial \ln W_p}{\partial \phi_p} + \tilde{\nu} N^{1/2} \left[\frac{L-2\delta}{L} \phi_m \frac{\partial \phi_m}{\partial \phi_g} + \frac{2\delta}{L} \phi_\delta \frac{\partial \phi_\delta}{\partial \phi_g} - \phi_p \right] \right] - (\tilde{\nu} N^{1/2}/2) [(L-2\delta) \phi_m^2 + 2\delta \phi_\delta^2 - L \phi_p^2] + \frac{8\pi N}{6^{2.5} s_0} \left[\phi_s \left(1 - \frac{u_{pp} \phi_s}{2kT} \right) + \ln(1-\phi_s) - \phi_s \frac{\partial \phi_s}{\partial \phi_g} \left(1 - \frac{u_{pp} \phi_s}{kT} - \frac{1}{1-\phi_s} \right) \right] \quad (29)$$

Subtracting the infinite separation limit of (29) yields the interaction potential.

For separations less than 2δ , we assume a flat segment profile so the solution of (3) is straightforward:

$$P(N, x|x') = P^0(N, x|x') [1 - \tilde{\nu} N^{1/2} \phi_g] \quad \text{for } L < 2\delta \quad (30)$$

with the resulting Helmholtz free energy per area (times Nl^2)

$$\frac{A}{kT} \frac{Nl^2}{A} = L \phi_g \left[-1 + \phi_g \frac{\partial \ln W_g}{\partial \phi_g} - \phi_p \frac{\partial \ln W_p}{\partial \phi_p} + \tilde{\nu} N^{1/2} [\phi_g - \phi_p] \right] - (\tilde{\nu} N^{1/2} L/2) [\phi_g^2 - \phi_p^2] + \frac{8\pi N}{6^{2.5} s_0} \left[\phi_s \left(1 - \frac{u_{pp} \phi_s}{2kT} \right) + \ln(1-\phi_s) - \phi_s \frac{\partial \phi_s}{\partial \phi_g} \left(1 + \frac{u_{pp} \phi_s}{kT} - \frac{1}{1-\phi_s} \right) \right] \quad (31)$$

Combining (29) and (31) and subtracting the limit of (29) as $L \rightarrow \infty$ give the interaction between the plates over the full range of separations.

Before calculating phase diagrams for these systems, examining the flat-plate potentials provides insight into

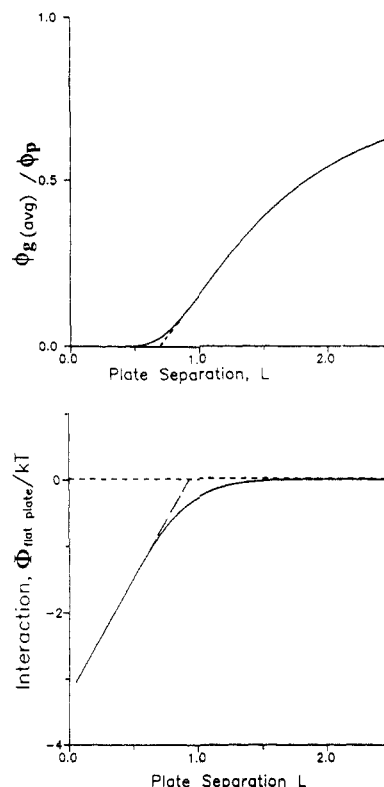


Figure 1. Approach of parallel plates immersed in nonadsorbing ($u_{pp} = \chi_s = 0$) ideal polymer solution with $N = 1000$. $\phi_p = 1$. (A, top) Average polymer volume fraction in the gap, ϕ_g . (B, bottom) Interaction potential. The dashed line represents the simple geometric approximation.

macroscopic behavior.

Interaction Potentials: Results. Figure 1 shows the interaction energy per coil area between two flat plates in the presence of nonadsorbing ideal polymer with bulk concentration $\phi_p = 1$ and separation scaled on the coil's end-to-end distance. (Recall that ϕ_p is based on R_g and hence may exceed unity when coils overlap.) The interaction is purely attractive, with the range comparable to the size of the polymer coil. Figure 1A shows almost complete exclusion of the polymer from the gap at a plate separation of 0.7, determined by extrapolating the linear portion of the curve to zero concentration. Once the gap is devoid of coils, the attraction increase linearly with decreasing separation, in keeping with the theory of Asakura and Oosawa (line with long dashes). Thus the force per area, the osmotic pressure of the bulk solution, is constant.

The Derjaguin approximation

$$\frac{\Phi_{\text{sphere}}}{kT} = \pi \frac{d_c}{N^{1/2} l} \int_{R-d_c}^{\infty} \frac{\Phi_{\text{fp}}(L)}{kT} dL \quad (32)$$

relates the interaction potential between spheres to the flat-plate potential, for $N^{1/2} l \ll d_c$, with R the center-to-center separation. Figure 2 demonstrates the effect of particle/polymer diameter ratio on the resulting sphere-sphere potential. Larger particles experience stronger depletion attractions, with the range constant relative to the polymer radius but decreasing relative to particle size, affecting phase behavior. For example, with particles large compared to the polymer coil, Gast⁵ predicted fluid-solid transitions, with longer range attractions inducing fluid-fluid separations.

Figure 3 illustrates the effect of sticker-wall adhesion on the partitioning between the bulk and gap, and the equilibrium interaction between the plates for ideal coils

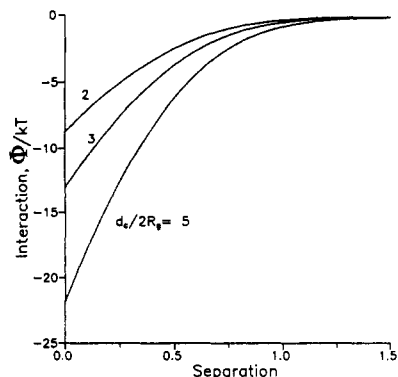


Figure 2. Effect of particle/polymer diameter ratio on the depletion attraction for ideal coils with $N = 1000$. $u_{pp} = \chi_s = 0$. $\phi_p = 1$.

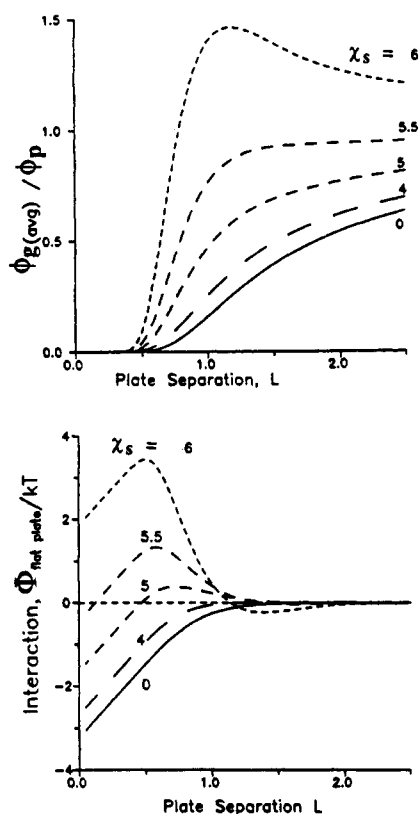


Figure 3. Effect of sticker-wall adhesion at full equilibrium conditions on (A, top) the average volume fraction of polymer in the gap and (B, bottom) the interaction potential between flat plates. Ideal coils, with $N = 1000$. $u_{pp}/kT = -1$. $\phi_p = 1$.

with $N = 1000$, $\phi_p = 1$, and $u_{pp} = -kT$. For the potentials shown here, the surface coverage is relatively low at all plate separations; hence stickers contribute their zero-coverage adhesion. The stickers do, however, significantly alter the partitioning of the chains between the gap and the bulk. The most attractive potentials occur without hydrophobes on the chain. As sticker-wall adhesion is increased, the attraction becomes shorter in range, eventually giving way to a repulsive barrier at sticker-wall strengths of $-5kT$. Strong hydrophobes ($\chi_s > 4$) hold coils in the gap at separations where nonassociating polymer would be excluded. Eventually, these chains are depleted, but not until the lingering coils contribute a repulsion, as the squeezing plates limit their internal degrees of freedom. With especially strong adsorption ($\chi_s > 6$) the gap concentration exceeds the bulk and a longer range "bridging" attraction appears at plate separations on the order of the end-to-end distance.

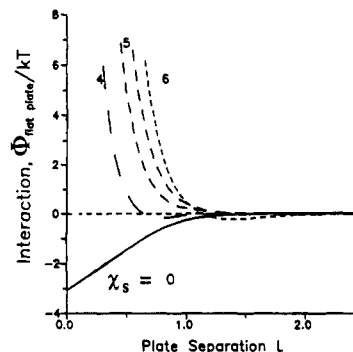


Figure 4. Effect of sticker-wall adhesion on the interaction potentials between flat plates at restricted equilibrium. Ideal coils, with $N = 1000$. $u_{pp}/kT = -1$. $\phi_p = 1$.

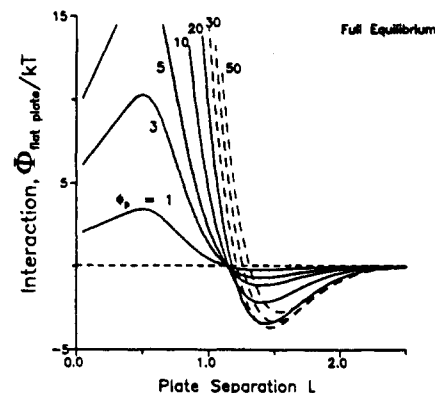


Figure 5. Effect of bulk polymer concentration on the bridging attraction between parallel plates at full equilibrium, with ideal coils. $N = 1000$. $\chi_s = 6$. $u_{pp}/kT = -1$.

It is worth emphasizing that even for equilibrium adsorption, the potential may contain high repulsive barriers, in contrast to that with adsorbing homopolymer. At each plate separation, equilibrium partitioning of the polymer gives a local minimum in $A(\phi_g)$ which can exceed that at infinite plate separation, producing a repulsion.

Quite a different situation occurs under restricted equilibrium conditions. As Figure 4 depicts, the long-range features of the potentials are identical with those of full equilibrium; however, the cores of the restricted potentials become increasingly repulsive as the sticker-wall adhesion increases. The adsorbed amount at infinite separation increases with sticker-wall adhesion, trapping more segments in the gap. As the plates approach, the free polymer eventually leaves the gap; however, the trapped coils become compressed, contributing an entropic repulsion at the core of the potential. The potentials predicted from the restricted mode everywhere equal or exceed those at full equilibrium, which adjusts the polymer concentration in the gap to minimize the free energy.

For strong hydrophobes, the strength of the bridging attraction is determined by the bulk polymer concentration and the surface coverage. Figure 5 shows this relationship for ideal chains with $\chi_s = 6$, $N = 1000$, and $u_{pp} = -kT$. As the polymer concentration in bulk solution is increased to $\phi_p = 25$, the depth of the attraction increases. However, further increases in polymer concentration reduce the attraction, since the surface becomes filled and bridged configurations contribute less to the partition function of the polymer in the gap. As more polymer adsorbs to the plates, the range of the core repulsion increases, but more gradually than at lower surface coverages. Note that the Gaussian treatment of the chains maintains the range of the repulsion at a single layer thickness, rather than two

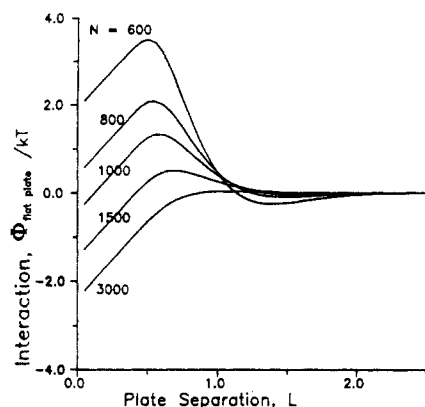


Figure 6. Effect of chain flexibility (N) for ideal coils on the interaction between parallel plates at full equilibrium. $\chi_s = 5.5$. $u_{pp}/kT = -1$. $\phi_p = 1$.

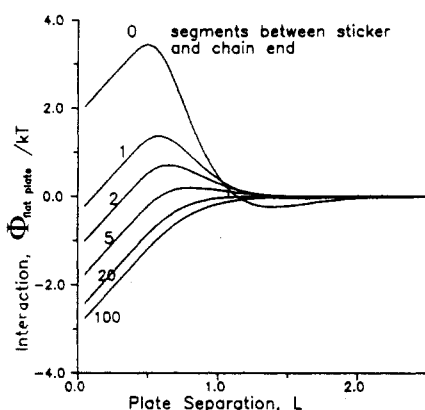


Figure 7. Effect of sticker position at full equilibrium on the interaction between parallel plates for ideal coils with $N = 1000$. $\chi_s = 6$. $u_{pp}/kT = -1$. $\phi_p = 1$.

brushes thick.

The loss of the bridging attraction occurs at unrealistically high polymer concentrations, $\phi_p > 90$, due to our Gaussian treatment of the polymer coils. When stickers nearly fill the surface, the attached Gaussian coils are equally packed, approaching bulk polymer conditions. Including even a small degree of nonideality gives restabilization at more realistic polymer concentrations as discussed below.

Flat-plate potentials for ideal chains with $\chi_s = 5.5$ and $u_{pp} = -kT$, in Figure 6, show that molecular weight can be as important as hydrophobe strength. Increasing molecular weight lessens the impact of the hydrophobes, recovering the volume restriction attraction. Short backbones sustain less entropic loss upon adsorption, so that hydrophobes are more effective, favoring bridging attraction.

The placement of the hydrophobe can be equally important as its strength. Figure 7 for $N = 1000$, $\chi_s = 6$, $u_{pp} = -kT$, $\phi_p = 1$, and ideal chains illustrates that the stickers appear strongest at the ends of a chain, producing an interaction potential with a strong repulsive core and a very slight bridging attraction. Moving the stickers even a few segments from the chain ends inhibits adsorption, thus recovering the volume restriction attraction in Figure 3 for very weak hydrophobes.

Thus far, we have discussed the effects of polymer chains on parallel-plate interactions for ideal chains only. The extension of the model to good solvents shows that segment-segment exclusion will significantly affect the interaction potentials. Before delving into our predictions for the effect of solvent quality, we first discuss the effects

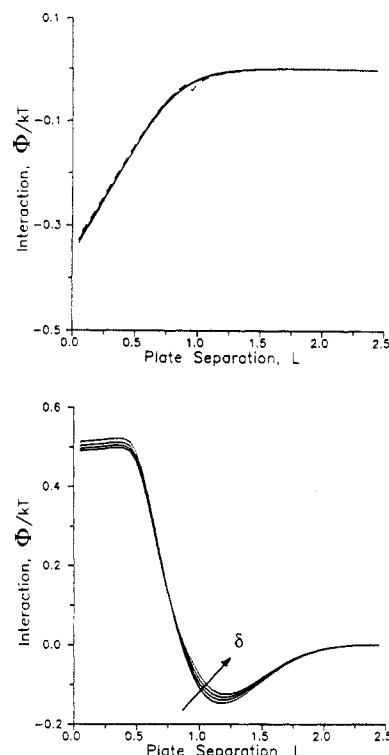


Figure 8. Effect of layer thickness on (A, top) depletion attraction with $u_{pp} = \chi_s = 0$, $\phi_p = 0.10$, and $N = 500$ and (B, bottom) bridging attraction with $\chi_s = 7$, $u_{pp}/kT = -1$, $\phi_p = 0.01$, and $N = 500$. In both $\nu = 0.03$ and $\delta = 0.30, 0.35, 0.40$, and 0.46 . (In (A) the dotted line signifies $\delta = 0.46$.)

of the layer thickness, δ , an adjustable parameter, on our predictions.

Figure 8 illustrates that for the extreme cases of depletion ($\chi_s = u_{pp} = 0$, $N = 500$, and $\phi_p = 0.1$) and bridging attraction ($\chi_s = 7$, $u_{pp} = -kT$, $N = 500$, and $\phi_p = 0.01$), δ may vary from 0.3 to 0.46 with little effect on the interaction potential. With sticker strengths between these extremes, the layer thickness affects the potentials in ways that are unclear and perhaps unphysical. For the depletion attraction, a small anomaly appears at $L = 2\delta$ for $\delta = 0.46$. For $L > 2\delta$, the region near the wall is devoid of chains, with $\phi_g \sim 0.08\phi_p$ at $L = 2\delta$. As $L \rightarrow 2\delta^+$, the free chains are forced into the shrinking region at the center of the gap, ultimately giving an infinite concentration at $x = \delta$.

Similar problems in the bridging attraction occur primarily in the repulsive core for $\delta = 0.46$ and do not interfere with the perturbation theory and phase diagrams. The "free chain effect" also occurs for $\delta = 0.3$ but is less visible since the concentration of free chains in the gap at $L = 0.6$ is negligible. Allowing free chains to penetrate the surface layer may avoid this problem. In the calculations to follow, we choose $\delta = 0.4$, comparable to the coil's radius of gyration.

Figure 9 shows the opposing effects of segment exclusion on volume restriction and bridging attractions for $\chi_s = 0$ and 7, respectively, $N = 500$, and $\delta = 0.40$. In the upper plot, segment-segment repulsions give stronger depletion attractions as ν increases the osmotic pressure of the bulk solution. The lower plot illustrates a deleterious effect on bridging, however, as chains do not crowd near a surface in a good solvent.

Figure 10 further shows that with significant segment-segment repulsion, $\nu = 0.02$, the bridging attraction that grows with ϕ_p at low concentrations diminishes well below the overlap concentration. In contrast to Figure 5, where sticker-sticker repulsion limits surface coverage and

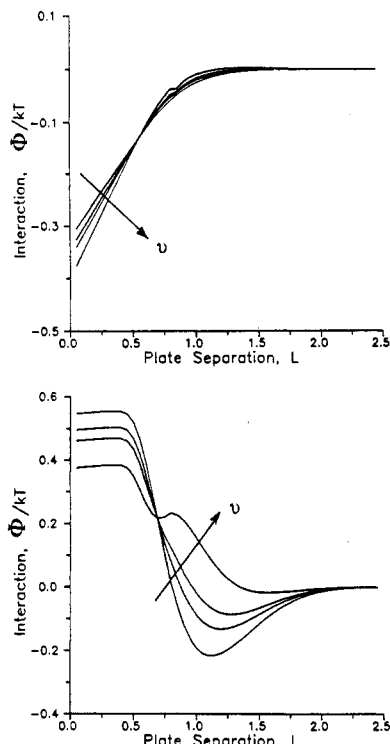


Figure 9. Effect of solvent quality on (A, top) depletion attraction with $u_{pp} = \chi_s = 0$ and $\phi_p = 0.10$ and (B, bottom) bridging attraction with $\chi_s = 7$, $u_{pp}/kT = -1$, and $\phi_p = 0.01$. In both cases $N = 500$, $\delta = 0.40$, and $\nu = 0.0, 0.03, 0.05$, and 0.10 .

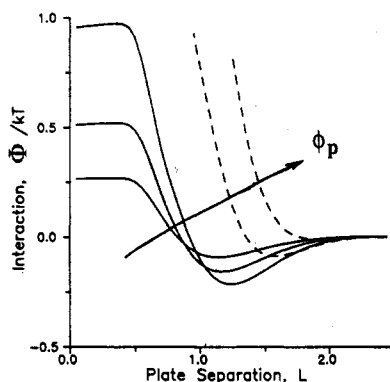


Figure 10. Effect of bulk polymer concentration on bridging attraction for $\chi_s = 7$, $u_{pp}/kT = -1$, $N = 1000$, $\delta = 0.40$, and $\nu = 0.02$. $\phi_p = 0.005, 0.01, 0.02, 0.05$, and 0.07 .

ultimately prevents bridging, segment-segment repulsions between coils just off the surface drive the restabilization. The surface coverage is low enough in Figure 10 that lateral sticker-sticker interactions within the surface have no effect on their adsorption strength.

From these interactions, one may anticipate general trends in the phase behavior of dispersions for certain polymer characteristics. It is well established that long-range attractions of the type in Figure 2 give broad fluid-fluid or fluid-solid transitions, depending on the particle size relative to the polymer. In the absence of attractions, hard spheres undergo a disorder-order transition from a dense fluid with $\phi = 0.50$ to an order solid of $\phi = 0.55$. The attraction broadens the narrow hard-sphere transition into an extensive two-phase region. Hence, eliminating the volume restriction attraction should stabilize the dispersions, except for the hard-sphere transition. The bridging attraction at strongly associative conditions should again give a large two-phase region, but with significant polymer in the particle-rich phase, since the polymer coats the particles at significant sticker-wall adhesions.

Phase Behavior

Theory. Phase behavior is determined by applying classical thermodynamic equilibrium conditions for one-component systems, i.e., equal pressures (Π) and particle chemical potentials (μ_c) in all phases:

$$\Pi^\alpha = \Pi^\beta \quad (33a)$$

$$\mu_c^\alpha = \mu_c^\beta \quad (33b)$$

We employ Barker-Henderson perturbation theory to calculate macroscopic properties, such as Helmholtz free energy from the interaction potentials, and Π and μ_c according to (12) and (13). The method²⁷ has been used by Gast et al.⁵ to model volume restriction flocculation for hard-sphere and electrostatically stabilized dispersions. The Helmholtz free energy of the dispersion, A , depends on that of a hard-sphere reference state, A° , and the hard-sphere radial distribution function, g° , to second order in the depth of the attraction:

$$\frac{A - A^\circ}{n_c kT} = 2\pi n_c \int_0^\infty \frac{\Phi(R)}{kT} g^\circ(R) R^2 dR - \pi n_c \left(\frac{\partial n_c}{\partial \Pi} \right)^\circ kT \int_0^\infty \left(\frac{\Phi(R)}{kT} \right)^2 g^\circ(R) R^2 dR + \dots \quad (34)$$

with n_c the particle number density. The diameter, d , of the hard-sphere reference state derives from the interaction potential as

$$d = \int_0^\sigma (1 - e^{-\Phi(R)/kT}) dR \quad (35)$$

with σ the point at which the potential equals zero. The properties of the hard-sphere reference state, A° and $(dn_c/d\Pi)^\circ$, are described by the Carnahan-Starling equation of state²⁸ for fluids ($\phi < 0.50$) and by Monte Carlo simulations at solid densities ($\phi > 0.55$). Pressure and Helmholtz free energy for the fluid depend on the volume fraction of particles of diameter d according to

$$Z^\circ(\text{fluid}) \equiv \frac{\Pi}{n_c kT} = \frac{1 + \phi + \phi^2 - \phi^3}{(1 - \phi)^3} \quad (36)$$

$$\frac{A^\circ - A^I}{kT} = \frac{\phi(4 - 3\phi)}{(1 - \phi)^2} \quad (37)$$

$$\phi = \frac{\pi n_c d^3}{6} \quad (38)$$

with A^I , the ideal-gas Helmholtz free energy. The equation of state for hard-sphere solids obtains from Hall's fit of Monte Carlo data via Padé approximants:²⁹

$$Z^\circ(\text{solid}) = 2.557696 + 0.1253077\beta + 0.1762393\beta^2 - 0.1053308\beta^3 + 2.818621\beta^4 - 2.921934\beta^5 + 1.118413\beta^6 + \frac{12 - 3\beta}{\beta} \quad (39)$$

$$\beta = 4(1 - \phi/0.07405)$$

The Helmholtz free energy of the reference solid is calculated by integrating pressure over volume and choosing the constant of integration to give the hard-sphere fluid-solid transitions between volume fractions of 0.50 and 0.55, respectively.

We use the fluid radial distribution function from the Percus-Yevick approximation (cf. McQuarrie²⁷) for hard spheres at fluid densities, following the approach of Wertheim³⁰ with the algebraic expressions of Smith and Henderson³¹ and the Verlet-Weiss³² corrections to improve agreement with Monte Carlo simulations. At solid densities, the hard-sphere radial distribution function is

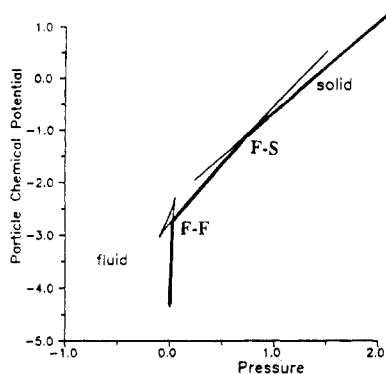


Figure 11. Particle chemical potential as a function of pressure for a system containing ideal polymer with $N = 1000$. $u_{pp} = \chi_s = 0$. $d_c/2R_g = 2$. $\phi_p = 0.19$.

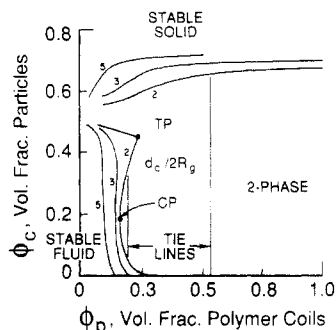


Figure 12. Effect of particle/polymer diameter ratio on the phase behavior of a dispersion containing nonadsorbing ($u_{pp} = \chi_s = 0$) ideal polymer with $N = 1000$. For $d_c/2R_g = 2$, the critical point (CP) and triple point (TP) are labeled, with two tie lines drawn. On the horizontal axis, the polymer volume fraction in the fluid is defined in terms of R_g .

described by the Kincaid-Weis fit to Weis's Monte Carlo simulations.³³ Detailed expressions are discussed elsewhere.⁵

Calculation Procedures. Phase diagrams are generated by varying the polymer and particle content of a dispersion to determine the compositions that satisfy (33a) and (33b). Recall that treating the particles as a one-component system prevents prediction of polymer partitioning, assuming the polymer solution to have the same concentration in the interstices of all phases. Thus, each polymer concentration corresponds to a tie line on the phase diagram. Using the graphical method in Figure 11, we generate phase envelopes one tie line at a time, first determining the interparticle potential, applying the perturbation theory to determine the Helmholtz free energy for $0.0 < \phi < 0.74$, and then deriving the corresponding pressures and chemical potentials, plotted in Figure 11 from (33). The upper branch represents the solid while the lower branch describes fluid densities. With constant polymer concentration, particle volume fraction varies along these curves in $\Pi-\mu_c$ space and the intersections indicate fluid-fluid (F-F) and fluid-solid (F-S) coexistence points, respectively. Most of the curve lies in the single-phase region (heavy lines), with the lighter lines describing two-phase systems. The dispersion will separate if the total composition matches a point on the light line. Because the curves are single valued in particle concentration, the system can lie in one of the two-phase regions, but not both.

Repeating the procedure in Figure 11 for different polymer concentrations traces out phase diagrams of the type in Figure 12 for ideal polymer, $N = 1000$, no hydrophobes, and varying $d_c/2R_g$. Particle volume fraction is plotted on the vertical axis with polymer volume fraction, based on radius of gyration, in the liquid surrounding the

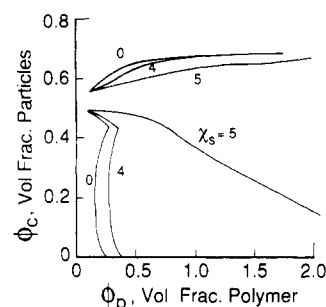


Figure 13. Effect of sticker-wall adhesion at full equilibrium on the phase behavior of a dispersion containing ideal associative polymer, with $N = 1000$. $u_{pp}/kT = -1$.

particles on the horizontal axis. The upper branch maps the equilibrium solid with the fluid curves below. One uses the diagram by first locating the overall composition. If this point lies inside the two-phase region, the vertical tie line (shown for two different polymer concentrations with $d_c/2R_g = 2$) gives the volume fractions of the coexisting phases. Note that the critical point (CP) of the fluid-fluid transition lies at the extreme left of the fluid envelope. With initial solids less than 0.50, the system remains stable at the lowest polymer concentrations; however, increasing the polymer concentration eventually moves the system into the two-phase fluid-fluid region. Further increases in polymer concentration beyond TP, the triple-point cusp, produce a light fluid in equilibrium with a solid. If the initial dispersion contains particle concentrations between 0.50 and 0.55, a fluid-solid transition will occur at all polymer concentrations, reflecting the limiting hard-sphere transition in the absence of polymer.

Phase Diagrams. The phase behavior is sensitive to particle/polymer size ratio, as demonstrated in Figure 12 for ideal chains, $N = 1000$, without hydrophobes. Larger particles, i.e., $d_c/2R_g > 3$, undergo exclusively fluid-solid transitions due to the shorter range of the attraction (recall Figure 2) relative to the particles. The fluid-fluid transition appears only for $d_c/2R_g < 3$.

Figure 13 illustrates the effects of hydrophobes at full equilibrium, for ideal chains with $N = 1000$, $u_{pp} = -kT$, and $0 < \chi_s < 5$. The phase behavior reflects the interactions of Figure 3A with the hydrophobes stabilizing against volume restriction flocculation. Figure 13 demonstrates that twice as much polymer with $-4kT$ hydrophobes is needed to induce flocculation compared to the nonassociating chains. With stronger hydrophobes, the effect is even more dramatic: The fluid-fluid transition is completely lost, with even higher polymer concentrations needed to induce the fluid-solid transition. At restricted equilibrium, the extensive two-phase region is lost when χ_s is large enough to give purely repulsive interaction potentials in Figure 4. Then, only the order-disorder transition occurs.

At sticker-wall adhesions exceeding $6kT$, the dispersion undergoes bridging flocculation and restabilization under both full and restricted conditions (Figure 14). Small particles tend to give fluid-fluid transitions at moderate concentrations with fluid-solid separations at higher polymer concentrations. Again, large particles ($d_c/2R_g > 3$) give exclusively fluid-solid transitions, requiring less polymer to induce flocculation initially and restabilizing at higher polymer concentrations. As anticipated, restabilization occurs at unrealistically high polymer concentrations, due to our Gaussian treatment of the chains. The phase boundaries in Figure 14 are nearly identical with those at restricted equilibrium conditions (not shown). So close is the resemblance that it would be

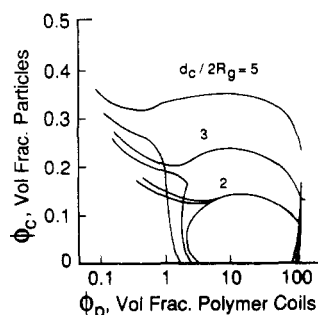


Figure 14. Effect of particle/polymer diameter ratio on the phase behavior of a dispersion containing ideal associative polymer, at full equilibrium. $N = 1000$. $u_{pp}/kT = -1$. $\chi_s = 6$. Bridging separation occurs under these conditions.

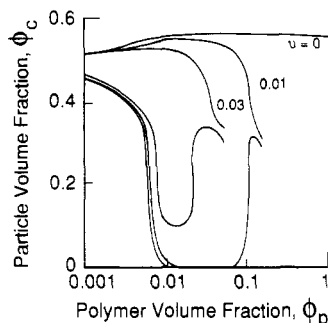


Figure 15. Effect of solvent quality on bridging flocculation for $\chi_s = 7$, $u_{pp}/kT = -1$, $N = 500$, $\delta = 0.40$, and $d_c/2R_g = 10$.

difficult to distinguish experimentally between the two scenarios of full and restricted equilibrium.

In Figure 15 we see the effect of solvent quality on bridging flocculation for $\chi_s = 7$, $u_{pp} = -kT$, $\delta = 0.4$, $N = 500$, and $d_c/2R_g = 10$. At Θ conditions without segment-segment exclusion, restabilization from surface saturation occurs well above the polymer overlap concentration. Though increasing segment-segment exclusion has little effect on the onset of bridging, restabilization occurs at lower concentrations in systems with significant segment-segment repulsions. In fact, bridging flocculation is not predicted for very good solvents ($\nu > 0.04$), except with stronger hydrophobes. Likewise with the conditions in Figure 15, attractions between smaller particles (i.e., $d_c/2R_g \sim 5$) are too weak to induce flocculation.

In Figure 16 we compare the predictions of the one-component model with Sperry's experiments,⁹ which determined the concentration of hydrophobically modified poly(ethylene oxide) (molecular weight 40 000) needed to flocculate a 0.30- μm poly(methyl methacrylate-butyl acrylate) copolymer latex containing $\phi_c = 0.25$. Polymer concentration is scaled as the dimensionless driving force for depletion flocculation, which goes as chain number density times $d_c/2R_g$. In the model, $N = 660$ is based on the characteristic ratio for PEO,²¹ with $\nu = 0.01$, $u_{pp} = -kT$, and χ_s varied on the horizontal axis. In the experiments, sodium lauryl sulfate was added to solvate the hydrophobic grafts on the associative thickener, decreasing the effective sticker strength through associations in solution and also competing with the PEO for adsorption sites on the latices.

At high surfactant concentrations the polymer induces a volume restriction flocculation. With decreasing surfactant concentration, the system becomes less susceptible to volume restriction flocculation, requiring more polymer to induce phase separation. This observation is consistent with the effect of hydrophobe strength in the theory. At very strong hydrophobe strengths ($\chi_s > 5.5$) in the one-component model, or with very little surfactant in Sper-

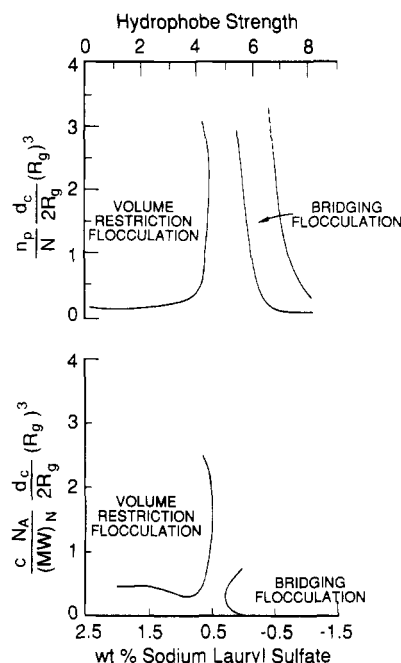


Figure 16. Comparison of theoretical predictions for the minimum polymer to flocculate a dispersion with $\phi_c = 0.25$ to Sperry's experiments with 0.30- μm poly(methyl methacrylate-butyl acrylate) copolymer latices. (A, top) Theory for $d_c/2R_g = 19$, $\chi_s = 7$, $u_{pp} = -kT$, $\nu = 0.01$, $\delta = 0.40$, and $N = 660$. (B, bottom) Experiments varying the amount of sodium dodecyl sulfate.

ry's experiments, the dispersion undergoes a bridging flocculation. The one-component theory predicts that the concentration to restabilize against bridging decreases with increasing hydrophobe strength, while Sperry's tests indicate the opposite: Decreased surfactant concentration results in higher PEO concentrations for restabilization. This conflict emphasizes that while surfactant decreases hydrophobe strength via associations in solution, it also reduces the latex surface available to the polymer.

Conclusions

We have presented a statistical mechanical treatment of Gaussian or slightly nonideal polymer chains containing associative end groups to predict the effects of these molecules on the phase behavior of colloidal dispersions. Considering the internal degrees of freedom in the chain and its affinity for the particle's surface facilitates calculating the interaction between two plates immersed in polymer solutions at full and restricted equilibrium conditions. The Derjaguin approximation, Barker-Henderson perturbation theory, and classical thermodynamic criteria for one-component systems yield the compositions of coexisting phases. Implicit in this treatment are the assumptions that (a) segment-segment exclusion has only a first-order effect on the polymer configuration and solution thermodynamics, (b) the polymer is smaller than the particle, (c) pairwise interactions dominate the thermodynamics, and (d) polymer aggregation and micellization are not significant. The last of these constraints is likely to be the most serious, with experiments indicating micellization in dilute polymer solutions.²⁰ We approach this problem in a previous paper to determine the concentrations at which a polymer solution containing only free coils is stable.

Many of the predictions from the one-component model presented here concur with the binary model.¹⁸ In the limit of weak sticker-wall adhesion, polymer-particle repulsions induce osmotic interparticle attractions that lead to phase separations at moderate polymer concentrations.

Increasing sticker-wall adhesion draws the polymer to the surface, stabilizing against volume restriction flocculation. With even stronger sticker-wall adhesions, bridged configurations induce attractions and phase separations not predicted by the mixture model, but observed experimentally. In addition to the chemical make-up of a hydrophobe, its placement within the polymer and the molecular weight of the backbone determine its affinity for the surface, with end-modified chains of low molecular weight being adsorbed most easily. Particle size relative to the polymer influences the nature of the phase transition and the minimum polymer needed to flocculate a dispersion. Large particles undergo fluid-solid transitions at relatively low polymer concentrations while smaller particles ($d_c/2R_g < 3$) can withstand more polymer before undergoing fluid-fluid transitions.

Segment-segment exclusion is important only at moderate polymer concentrations, greater than 0.1 times the overlap concentration. Phenomena that occur at more dilute conditions, such as the onset of bridging, are virtually unaffected by segment-segment interactions. Since restabilization occurs beyond the overlap concentration with ideal coils, segment-segment exclusion becomes significant, reducing the restabilization concentration to realistic values. As previously established, segment-segment repulsions in nonadsorbing or weakly adsorbing polymer favor volume restriction flocculation by increasing the osmotic pressure of the bulk solution.

The general trends predicted by this one-component approach compare favorably with Sperry's observations for the minimum polymer concentration to flocculate dispersions containing varying surfactant concentrations. In a subsequent paper, we will make a quantitative comparison with our experiments.

Acknowledgment. This research was funded by a grant from Hercules/Aqualon and a National Science Foundation Fellowship to M.M.S.

References and Notes

- (1) Vincent, B. *Colloids Surf.* **1987**, *24*, 269-83.
- (2) Sperry, P. R. *J. Colloid Interface Sci.* **1984**, *99*, 97-108.
- (3) Gast, A. P.; Russel, W. B.; Hall, C. K. *J. Colloid Interface Sci.* **1986**, *109*, 161-71.
- (4) Patel, P.; Russel, W. B. *J. Colloid Interface Sci.* **1989**, *131*, 192-200.
- (5) Gast, A. P.; Russel, W. B.; Hall, C. K. *Faraday Discuss. Chem. Soc.* **1983**, *76*, 189-201.
- (6) Asakura, S.; Oosawa, F. *J. Polym. Sci.* **1958**, *33*, 183-92.
- (7) Vrij, A. *Pure Appl. Chem.* **1976**, *48*, 471-83.
- (8) Rossi, G.; Pincus, P. A. *Macromolecules* **1989**, *22*, 276-83.
- (9) Sperry, P. R.; Thibault, J. C.; Kostansek, E. C. *Adv. Org. Coat. Sci. Technol. Ser.* **1985**, *9*, 1-11.
- (10) de Hek, H.; Vrij, A. *J. Colloid Interface Sci.* **1981**, *84*, 409-22.
- (11) Scheutjens, J. M. H. M.; Fleer, G. J. *ACS Symp. Ser.* **1984**, *No. 240*, 245-63.
- (12) Scheutjens, J. M. H. M.; Fleer, G. J. *J. Phys. Chem.* **1979**, *83*, 1619-35; **1980**, *84*, 178-90.
- (13) de Gennes, P.-G.; Pincus, P. *Phys. Lett. (Paris)* **1983**, *44*, L241.
- (14) Joanny, J. F.; Leibler, L.; de Gennes, P.-G. *J. Polym. Sci., Polym. Phys. Ed.* **1979**, *17*, 1073-84.
- (15) de Gennes, P.-G. *Adv. Colloid Interface Sci.* **1987**, *27*, 189-209.
- (16) Ploehn, H. J.; Russel, W. B.; Hall, C. K. *Macromolecules* **1988**, *21*, 1075-85.
- (17) Luckhman, P. F.; Klein, J. *Macromolecules* **1985**, *18*, 721-28.
- (18) Santore, M. M.; Russel, W. B.; Prud'homme, R. K. *Macromolecules* **1989**, *22*, 1317-25.
- (19) de Gennes, P.-G. *Macromolecules* **1982**, *14*, 1637-49.
- (20) Gelman, R. A.; Barth, H. G. *Adv. Chem. Ser.* **1985**, *No. 213*, 101-10.
- (21) Tanford, C. *The Hydrophobic Effect: Formation of Micelles and Biological Membranes*, 2nd ed.; Wiley: New York, 1980; Chapter 1.
- (22) Brandrup, J.; Immergut, E. H., Eds. *Polymer Handbook*, 2nd ed.; Wiley: New York, 1975.
- (23) Russel, W. B.; Saville, D. A.; Schowalter, W. R. *Colloidal Dispersions*; Cambridge University Press: New York, 1989; Chapter 6.
- (24) Dolan, A. K.; Edwards, S. F. *Proc. R. Soc. London A* **1974**, *337*, 509-16.
- (25) Helfand, E. *J. Chem. Phys.* **1975**, *62*, 999-1005.
- (26) Evans, E. A. *Macromolecules* **1989**, *22*, 2277-86.
- (27) McQuarrie, D. A. *Statistical Mechanics*; Harper and Row: New York, 1976.
- (28) Carnahan, N. F.; Starling, K. E. *J. Chem. Phys.* **1970**, *53*, 600-1.
- (29) Hall, C. K. *J. Chem. Phys.* **1975**, *57*, 2252-4.
- (30) Wertheim, M. S. *Phys. Rev. Lett.* **1963**, *10*, 321-3.
- (31) Smith, W. R.; Henderson, D. *Mol. Phys.* **1970**, *19*, 413-8.
- (32) Verlet, L.; Weis, J. J. *Phys. Rev. A* **1972**, *5*, 939-52.
- (33) Weis, J. J. *Mol. Phys.* **1974**, *28*, 187-95.